Sarkar, S., Prasad, S., Wilkes, H., Riedel, N., Stebich, M., Basavaiah, N., Sachse, D. (2015): Monsoon source shifts during the drying mid-Holocene: Biomarker isotope based evidence from the core 'monsoon zone' (CMZ) of India. - *Quaternary Science Reviews*, *123*, p. 144-157.

DOI: http://doi.org/10.1016/j.quascirev.2015.06.020

Monsoon source shifts during the drying mid-Holocene: biomarker isotope based evidence from the core 'monsoon zone' (CMZ) of India

Saswati Sarkar[a], Sushma Prasad[a], Heinz Wilkes[b], Nils Riedel[c], Martina Stebich[c], Nathani Basavaiah[d], Dirk Sachse[a,e*]

[a]Institute for Earth- and Environmental Science, University of Potsdam, Karl-Liebknecht-Straße 24-25, 14476 Potsdam, Germany.

[b]Helmholtz Centre Potsdam GFZ German Research Centre for Geosciences, Section 4.3, Organic Geochemistry, Telegrafenberg, D-14473 Potsdam, Germany.

[c]Senckenberg Research Institute, Research Station of Quaternary Palaeontology, Am Jakobskirchhof 4, D-99423 Weimar, Germany.

[d]Indian Institute of Geomagnetism, New Panvel, Navi Mumbai, India.

[e]Helmholtz Centre Potsdam GFZ German Research Centre for Geosciences Section 5.1, Geomorphology, Organic Surface Geochemistry Lab, Telegrafenberg, D-14473 Potsdam, Germany.

[*]Corresponding author: dirk.sachse@gfz-potsdam.de, Phone: +49-331-288-28823

Abstract

A better understanding of past variations of the Indian Summer Monsoon (ISM), that plays a vital role for the still largely agro-based economy in India, can lead to a better assessment of its potential impact under global climate change scenarios. However, our knowledge of spatiotemporal patterns of ISM strength is limited due to the lack of high-resolution, continental paleohydrological records. Here, we reconstruct centennial-scale hydrological variability during the Holocene associated to changes in the intensity of the ISM based on a record of lipid biomarker abundances and compound-specific stable isotopic composition of a 10 m long sediment core from saline-alkaline Lonar Lake, situated in the core 'monsoon zone' of central India.

We identified three main periods of distinct hydrology during the Holocene in central India. The period between 10.1 and 6 cal. ka BP was likely the wettest during the Holocene. Lower average chain length (ACL) index values (29.4 to 28.6) and negative $\delta^{13}C_{wax}$ values (–34.8‰ to –27.8‰) of leaf wax *n*-alkanes indicate the dominance of woody C_3 vegetation in the catchment, and negative δD_{wax} values (concentration weighted average) (–171‰ to –147‰) suggest a wet period due to an intensified monsoon. After 6 cal. ka BP, a gradual shift to less negative $\delta^{13}C_{wax}$ values (particularly for the grass derived *n*-C_{31}) and appearance of the triterpene lipid tetrahymanol, generally considered as a marker for salinity and water column stratification, mark the onset of drier conditions. At 5.1 cal. ka BP an increasing flux of leaf wax *n*-

alkanes along with the highest flux of tetrahymanol indicate a major lowering of the lake level. Between 4.8 and 4 cal. ka BP, we find evidence for a transition to arid conditions, indicated by high and strongly variable tetrahymanol flux. In addition, a pronounced shift to less negative $\delta^{13}C_{wax}$ values, in particular for *n*-C_{31} (–25.2‰ to –22.8‰), during this period indicates a change of dominant vegetation to C_4 grasses. In agreement with other proxy data, such as deposition of evaporite minerals, we interpret this period to reflect the driest conditions in the region during the last 10.1 ka. This transition led to protracted late Holocene arid conditions after 4 ka with the presence of a permanent saline lake, supported by the sustained presence of tetrahymanol and more positive average δD_{wax} values (–122‰ to –141‰). A late Holocene peak of cyanobacterial biomarker input at 1.3 cal. ka BP might represent an event of lake eutrophication, possibly due to human impact and the onset of cattle/livestock farming in the catchment.

A unique feature of our record is the presence of a distinct transitional period between 4.8 and 4 cal. ka BP, which was characterized by some of the most negative δD_{wax} values during the Holocene (up to –180‰), when all other proxy data indicate the driest conditions during the Holocene. These negative δD_{wax} values can as such most reasonably be explained by a shift in moisture source area and/or pathways or rainfall seasonality during this transitional period. We hypothesize that orbital induced weakening of the summer solar insolation and associated reorganization of the general atmospheric

circulation, as a possible southward displacement of the tropical rainbelt, led to an unstable hydroclimate in central India between 4.8 and 4 ka.

Our findings shed light onto the sequence of changes during mean state changes of the monsoonal system, once an insolation driven threshold has been passed, and show that small changes in solar insolation can be associated with major hydroclimate changes on the continents, a scenario that may be relevant with respect to future changes in the ISM system.

Keywords: Indian Summer Monsoon; Holocene; Lonar Lake; lipid biomarkers; compound-specific stable isotopic composition

1. Introduction

The Indian monsoon is an important component of the Earth's climate system. More than 15% of the world's population lives in areas affected by the monsoon. Rainfall from the Indian summer monsoon (ISM) was and still is largely responsible for the development and sustenance of the largely agro-based economy on the Indian subcontinent (Gadgil et al., 2005). The ISM is predicted to change under global warming (Goswami et al., 2006; Malik et al., 2012), but the magnitude and regional consequences of these changes are uncertain (Ghosh et al., 2011). Thus, knowledge of the magnitude and timing of past ISM variation on regional scales is crucial to better predict its response to anthropogenic climate change. Marine as well

as continental records, mainly from the peripheral realm of the ISM, have indicated a largely insolation-driven smooth transition from Early Holocene wet to Late Holocene arid conditions (Fleitmann et al., 2003; Gupta et al., 2003; Fleitmann et al., 2007; Ponton et al., 2012). However, few high-resolution Holocene records from continental archives, such as speleothems exist, but these are not continuous and not from the core 'monsoon zone' (CMZ), (MZ: Gadgil, 2003). As such, it is difficult to evaluate the nature of this mid-Holocene transition on land.

Here, we reconstructed centennial-scale hydrological variability associated to changes in the intensity of the ISM over the Holocene, based on aquatic and terrestrially sourced lipid biomarkers and their stable carbon and hydrogen isotopic composition ($\delta^{13}C$ and δD values), of a 10 m long sediment core from saline-alkaline Lonar Lake (Fig. 1). Lonar Lake lies in the CMZ in central India and is currently the only lake providing a continuous Holocene sediment record in this region (Prasad et al., 2014).

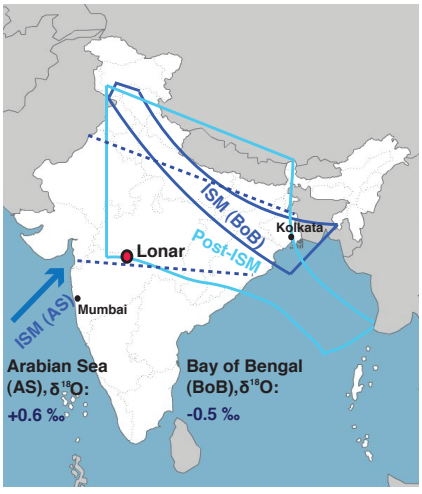

Fig. 1. Envelopes in dark and light blue represent storm-tracks from Bay of Bengal (BoB) in monsoon and post-monsoon, respectively; the smaller arrow represents the Arabian Sea (AS) branch (modified after Sengupta and Sarkar, 2006). Location of Lonar crater lake in the 'monsoon zone' (Gadgil, 2003) marked by the blue dashed line. The variations of rainfall over this region show a strong correlation with the variations of the Indian summer monsoon rainfall (Gadgil, 2003) and therefore can be considered as representative area for Indian summer monsoon.

Modern seawater $\delta^{18}O$ values are indicated for Arabian Sea and Bay of Bengal (from Kumar et al., 2010).

The overall temporal development of the ISM during the Holocene is well known for the Indian Ocean basin based on the analysis of several marine sediment cores (Fleitmann et al., 2003; Gupta et al., 2003; Fleitmann et al., 2007). These studies revealed a significant decrease in monsoon strength around 5-4.5 cal. ka BP and protracted arid conditions during the late Holocene. In contrast, the associated changes in continental hydrology and ecosystem changes are difficult to assess. In our present study we apply organic geochemical proxies on a sediment core from the precipitation fed closed-basin Lonar Lake, to assess the consequences of the change in ISM mean state at around 5-4 ka, directly on the Indian subcontinent.

From previous multi proxy investigations on the same sediment core from Lonar Lake, which we investigate here, two phases of severe aridity (between 4.6-3.9 and 2-0.6 cal. ka BP) have been identified following an early Holocene wet phase (Prasad et al., 2014). In addition, these available data on Holocene

136 climate changes (Prasad et al., 2014) as well as investigations of the modern
137 catchment and lake environment (Menzel et al., 2013; Basavaiah et al., 2014;
138 Sarkar et al., 2014) provide us with a well-constrained modern framework in
139 which the biomarker and isotope data can be interpreted.
140 In this study we specifically focus on the transition from wet to dry
141 conditions during mid-Holocene to obtain additional information on monsoon
142 hydrology during the change from early Holocene wet to late Holocene dry
143 conditions.
144
145 *1.1 Organic geochemical proxies as indicators of paleoclimate changes*
146 *1.1.1 Biomarkers*
147 The potential to separate the aquatic and terrestrial response of lake
148 ecosystem changes using techniques such as elemental and isotope
149 geochemical proxies is limited since bulk sediments represent a mixture of
150 many components (Krishnamurthy et al., 1995). Due to higher source-
151 specificity of individual compounds relative to bulk material/sediment, lipid
152 biomarkers and their stable isotope ratios are increasingly applied to lake
153 sediment archives for investigating environmental changes (Castañeda and
154 Schouten, 2011) in the lake and catchment ecosystems as well as hydrology
155 over time (Schwark et al., 2002; Romero-Viana et al., 2012). For example,
156 long chain *n*-alkanes (with 27 to 35 carbon atoms) are produced as leaf wax
157 constituents of terrestrial higher plants (Eglinton and Hamilton, 1967;

158 Cranwell et al., 1987). Changes in the abundance of leaf wax compounds can
159 be used mainly as proxies for transport of terrigenous OM to the lake
160 (Meyers, 2003). For the aquatic component, compositional variations in
161 aquatic lipids can be used to assess changes in the lake ecosystem. For
162 example, variations in the abundance of the cyanobacterial biomarkers, such
163 as *n*-heptadecane can be used as proxies for changes in primary productivity.
164
165 *1.1.2 Carbon and hydrogen isotopes*
166 The analysis of the stable carbon and hydrogen isotopic composition of
167 these biomarker compounds (expressed as $\delta^{13}C$ and δD values) has emerged
168 as a powerful tool that can provide detailed insights into ecosystem and
169 hydrological development (Tierney et al., 2008; Rach et al., 2014).
170 With the help of $\delta^{13}C$ values of long chain *n*-alkanes ($\delta^{13}C_{wax}$) changes in
171 vegetation (e.g. C_3 trees/C_4 grasses) can be detected (Sinninghe Damsté et al.,
172 2011), since $\delta^{13}C_{wax}$ values clearly differ between C_3 and C_4 plants
173 (Rommerskirchen et al., 2006b; Tipple and Pagani, 2010) due to differences in
174 carbon assimilation pathways (Eglinton and Eglinton, 2008). $\delta^{13}C$ values of
175 aquatic biomarkers can in turn be used to asses the carbon source of
176 individual compounds and carbon cycling through the ecosystem. $\delta^{13}C$ values
177 of lipids from primary producers, such as cyanobacteria, reflect the carbon
178 isotopic composition of DIC (dissolved inorganic carbon), which can be
179 affected by factors such as productivity or alkalinity (salinity) in the lake.

180 δD values of biomarkers are increasingly applied as a proxy to detect
181 changes in paleohydrology, as the ultimate hydrogen source of any
182 photosynthetic organism is environmental water. As such, δD values of leaf
183 wax biomarkers (δD_{wax}) can be used to detect changes in the processes that
184 affect the isotopic composition of precipitation, such as moisture source or
185 rainfall amount. δD values of biomarkers derived from aquatic organisms in
186 general also record the δD values of the water source used by the organism,
187 but can additionally be affected by processes such as organism growth rate
188 and more importantly the salinity of the water (Sachs, 2014).
189 As such the stable C and H isotopic composition of terrestrial and aquatic
190 lipid biomarkers is a powerful proxy to document the change in hydrology
191 and ecosystem of the lake and its catchment area.
192

193 **2. Material and methods**

194 *2.1 Study site, modern hydrology and vegetation*

195 Lonar Lake in central India (19°58'N, 76°30'E; Buldhana district,
196 Maharashtra State, India) lies within a small crater (diameter: 1.8 km;
197 depth: 150 m) and was formed by a meteorite impact on the Deccan trap
198 basalts (Fredriksson et al., 1973). The site is extensively described in
199 Basavaiah et al. (2014), Prasad et al. (2014) and Sarkar et al. (2014).
200 Briefly, the slopes of the inner rim wall of the crater vary from 30° in the
201 west and southwest to 15°-18° in the east. Quaternary deposits covering

basalts accumulated below the upper sparsely vegetated slopes of the inner crater. Lakeward these deposits become undifferentiated within the dense forest. A network of rills and gullies cuts the walls of the crater while in the NE a deeply incised channel named Dhara Canyon occurs. The outflow from the Dhara Canyon has built an alluvial fan.

Lonar Lake is small (diameter: 1.2 km; depth: 5 m) and alkaline–saline (pH 10.5, salinity 10.5; La Touche, 1912; Jhingran and Rao, 1958; Nandy and Deo, 1961). The lake is located in the semi-arid region of central India, with an average annual rainfall of 760 ± 50 mm. Two general climatic periods, due to seasonality in the monsoon system, are observed: (i) a wet season from June to the end of September (summer monsoon/southwest monsoon), with an average rainfall of 670 ± 40 mm and (ii) a dry season from early October to June.

Belts of thornshrub and dry deciduous mixed forest characterize the crater rim. Although the existing vegetation has been altered by human activities, modern vegetation at Lonar crater can be described as tree savannah (Riedel et al., 2015), compromising a woody plant cover and a continuous C_4-grass understory. For a detailed description of the modern vegetation see Riedel et al. (2015). The aquatic biocenosis predominantly consists of floating cyanobacterial mats and emergent macrophytes, which are abundant mainly near an alluvial fan in the NE of the crater.

224 *2.2 Sediment core and age model*

225 In May-June 2008 a 10 m long composite core was retrieved from Lonar
226 Lake during a joint scientific expedition between IIG, Mumbai and GFZ,
227 Potsdam. The core was retrieved at a water depth of 5.4 m, using a UWITEC
228 Sediment Piston corer (Anoop et al., 2013; Prasad et al., 2014).

229 The core chronology is based on 19 ^{14}C AMS dates on terrestrial fragments
230 (wood, leaf, twigs), carbonate (gaylussite) crystals, and bulk sediment from
231 the core (Fig. 2) (Anoop et al., 2013; Prasad et al., 2014). The radiocarbon
232 dates on terrestrial fragments and gaylussite crystal are stratigraphically
233 consistent indicating absence of reworked terrestrial fragments. Paired
234 radiocarbon dates obtained on bulk sediments and terrestrial fragments at
235 the same depth mostly showed agreement within one standard deviation. The
236 apparent "older" dates for few of the bulk sediments could be potentially
237 caused by hard water effect (Fontes et al., 1996; Björck and Wohlfarth, 2001).
238 Due the absence of carbonate rocks in the catchment, the older dates on bulk
239 sediments were attributed to the lack of equilibration with the atmosphere
240 due to high salinity, stratification, and alkalinity in the lake (Prasad et al.,
241 2014). After the removal of outliers, calibration was done with the remaining
242 dates using the OxCal programme (Bronk Ramsey, 2008) using the
243 INTCAL04 and NH3 curves.

244

245 The core was comprised largely of calcareous clay. The core was laminated
246 with clay (intercalation of organic) and calcareous between 11.2-9 cal. ka BP

(Prasad et al., 2014). The most significant lithological characteristic of the core was the presence of evaporitic gaylussite (Na_2CO_3. $CaCO_3$. $5H_2O$) crystals in calcareous silty clay in two zones: mid (4.6-3.9 cal. ka BP) and upper (2-0.6 cal. ka BP).

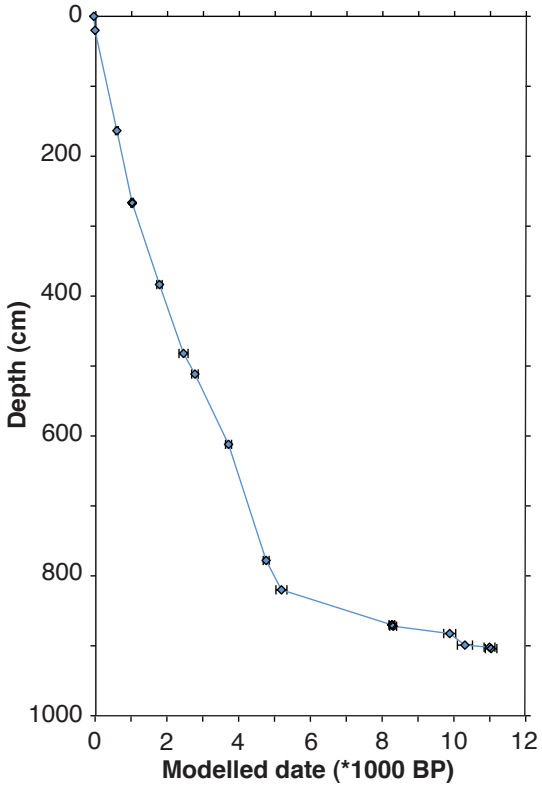

Fig. 2. Modelled ages (along with uncertainty) and depth from Lonar samples, adapted from (Anoop et al., 2013; Prasad et al., 2014).

2.3 Sample preparation and lipid biomarker analysis

For extraction of lipid biomarkers, 2 cm thick samples were taken from the sediment core for every 20 cm, resulting in 44 samples. Later 26 additional subsamples were included to improve sampling resolution during the

transitional period (4.8-4 cal. ka BP) and also the early Holocene period. For transitional period samples were taken for every 5-10 cm. In order to identify onset of transitional period (5.6-5.2 cal. ka BP), 1 cm thick samples were taken for every 1 cm. Samples represented a time span ranging from 8-20 years until 5.1 cal ka to 60-120 years in older sediments.

Ca. 2-4 g of sample, freeze-dried and homogenised, were extracted using an accelerated solvent extractor (Dionex ASE 350) with a mixture of dichloromethane (DCM)/methanol (9:1) at 100 °C and 103 bar (1500 psi) for 15 min in 2 cycles. After removal of elemental sulphur (passing through activated copper pipette columns) and addition of internal standards (5α-androstane, 5α-androstan-3ß-ol and erucic acid) the total extracts were separated on SPE silica gel columns (ca. 2 g of silica gel 60, 230-400 mesh) into three fractions of different polarity, namely an aliphatic hydrocarbon (eluted with 10 ml of *n*-hexane), an alcohol (eluted with 15 ml of DCM/acetone (9:1)) and a fatty acid fraction (eluted with 10 ml of DCM/methanol (5:1)).

Major alcohols, like tetrahymanol, were present in very high concentrations and could be analyzed without derivatization on our GC-MS system. Fraction one and two (containing aliphatic hydrocarbons and alcohols, respectively) were measured on a GC-FID/MSD system for compound identification and quantification. The GC-FID/MSD system consisted of an Agilent 7890A gas chromatograph equipped with a flame

304 ionization detector (FID) and an Agilent 5975C mass selective detector. The
305 system used a programmable temperature vaporization (PTV) inlet with split
306 injection (5:1), a capillary column (Agilent DB-5MS) (length 30 m, inner
307 diameter 0.25 mm and film thickness 0.25 μm) with helium as carrier gas. 1
308 μl of the sample was injected into the GC. The temperature of the injector
309 was 70 °C and after 2.5 min the temperature was increased at 720 °C/min to
310 300 °C; while the temperature of the GC oven was kept constant for 2 min at
311 70 °C initially. Subsequently the oven was heated to 280 °C at 7 °C/min and
312 then to 320 °C at 3 °C/min (15 min isothermal). Identification of compounds
313 was based on comparison of mass spectra with published data.
314
315 *2.4 Compound specific stable carbon and hydrogen isotope analysis*
316 The stable isotope composition of long chain *n*-alkanes was measured on 32
317 samples (for $\delta^{13}C$) and 36 samples (for δD). Since the study focus was on the
318 analysis of *n*-alkane δD values, not all samples could be analysed for their
319 $\delta^{13}C$ values as well, since sample material was exhausted. The stable isotope
320 composition of *n*-heptadecane could be determined on 27 samples (for $\delta^{13}C$)
321 and 24 samples (for δD). The stable isotope composition of tetrahymanol was
322 measured on 8 samples (for $\delta^{13}C$, δD).
323 The stable carbon isotope composition ($\delta^{13}C$) of biomarkers was measured
324 on a GC system (Agilent 6890N) coupled via combustion interface (GC-C III),
325 to a Thermo Scientific MAT 253 isotope ratio mass spectrometer (GC-irm-

MS). The system was equipped with a programmable temperature vaporization (PTV) inlet using split injection (1:1) and a fused silica capillary column (Agilent Ultra1) (length 50 m, inner diameter 0.2 mm and film thickness 0.33 μm). Helium was used as carrier gas. 1-3 μl of the sample were injected into the GC. The temperature (T) programs for the injection and GC oven/column were as follows:

PTV injector T-program: 230 °C (starting-T.), with 700 °C/ min up to 300 °C (hold for the complete run); Oven T-program: 40 °C (starting-T.) hold for 2min. with 4 °C/ min up to 300 °C (hold for 45 min).

For tetrahymanol, the system was equipped with a PTV inlet using split injection (1:1) and a fused silica capillary column BPX5 (length 50 m, inner diameter 0.2 mm and film thickness 0.25 μm). Helium was used as carrier gas. 3 μl of the sample were injected into the GC. The temperature (T) program for GC oven/column was as follows: 80 °C (starting-T.) hold for 1 min, with 15 °C/ min up to 250 °C, 1 °C/ min up to 310 °C (hold for 15 min).

GC-irm-MS analyses were run in triplicate. Calibration of isotope analysis was performed by injecting several pulses of CO_2 at the beginning and at the end of each GC run. Isotopic ratios are expressed as $\delta^{13}C$ values in per mil. $\delta^{13}C$ values of compounds measured in laboratory reference scale are converted to the Vienna Pee Dee Belemnite (V-PDB) scale using a linear regression function derived from the relationship of measured values and known values in V-PDB scale, for the compounds of a certified standard

between sample runs. The average standard deviation for standards over sequences was between 0.5 and 1.8 and for samples it was 0.5.

The stable hydrogen isotope composition (δD) of biomarkers was measured on a GC system (Agilent 6890N) coupled via pyrolysis interface to a Thermo Scientific Delta V Plus isotope ratio mass spectrometer (GC-irm-MS). The system was equipped with a PTV inlet using split injection (1:3) and a fused silica capillary column (Agilent Ultra1) (length 50 m, inner diameter 0.2 mm and film thickness 0.32 μm). Helium was used as carrier gas. 1-3 μl of the sample were injected into the GC. The temperature (T) programs for the injection and GC oven/column were as follows: Injector T-program: 230 °C (starting-T.), with 700 °C/ min up to 300 °C (hold for the complete run); Oven T-program: 40 °C (starting-T.) hold for 2min. with 4 °C/ min up to 300 °C (hold for 45 min).

For tetrahymanol, the system was equipped with a PTV inlet using split injection (1:1) and a fused silica capillary column (DB-FFAP) (length 60 m, inner diameter 0.25 mm and film thickness 0.25 μm). Helium was used as carrier gas. 3 μl of the sample were injected into the GC. The temperature (T) program for GC oven/column was as follows: 80 °C (starting-T) hold for 1 min, with 15 °C/ min up to 250 °C, 1 °C/ min up to 310 °C (hold for 15 min).

GC-irm-MS analyses were run in triplicate. Calibration of isotope analysis was performed by injecting several pulses of H_2 at the beginning and at the end of each GC run. Isotopic ratios are expressed as δD values in per mil. δD

values of compounds measured on the laboratory reference scale were converted to the Vienna Standard mean ocean (VSMOW) scale using a linear regression function derived from the relationship of measured values and known values of a certified standard (Mix A obtained from Arndt Schimmelmann, University of Indiana) between sample runs. The average standard deviation for standards and samples was around 3.

2.5 Precipitation, isotope data and backward trajectory analysis

Currently stable isotope data for precipitation are not available from the Lonar region but from the adjacent Sagar region (23°49'N, 78°45'E, 551 m a.s.l.), Madhya Pradesh (ca. 486 km NE of Lonar). Monthly rainfall data for the Sagar station (WMO code: 42671) is archived in the database of the Global Historical Climate Network (GHCN version 2), available at Climate Explorer of the Royal Netherlands Meteorological Institute (climexp.knmi.nl). Rainfall isotope data from Sagar is provided by IAEA/WMO (Global Network of Isotopes in Precipitation GNIP database; isohis.iaea.org) and also published in Kumar et al. (2010).

In order to determine the moisture source areas and their isotope fingerprint for Sagar an ensemble of backward air mass trajectories has been calculated using the Hybrid Single-Particle Lagrangian Integrated Trajectories (HYSPLIT) ARL trajectory tool database of NOAA. Trajectories for time periods of 96 h were computed at the lower troposphere (1500 m

392 a.s.l.) for the pre-monsoon, the monsoon (ISM), and the post-monsoon
393 seasons, for the years with existing precipitation isotopes data (2003 to 2005).
394
395 *2.6 Pollen analysis*
396 Pollen analysis was undertaken on 125 samples representing a temporal
397 resolution of 100 to 150 years from 9.1 to 5 cal. ka BP and 40 years between 5
398 and 0 cal. ka BP. Sediment samples were prepared using KOH; HCL; HF and
399 hot acetolysis-mixture. All samples were sieved with 200 and 5 µm mesh
400 gauze. At least 600 pollen grains were counted per sample. Identification of
401 palynomorphs is based on Nayar (1990); Tissot et al. (1994); the web-based
402 pollen atlas for the Australasian realm (APSA Members 2007); and the pollen
403 collection for south Asia at Senckenberg Research Station of Quaternary
404 Palaeontology, Weimar, Germany.
405
406 **3. Results**
407 *3.1 Higher terrestrial plant biomarkers*
408 *3.1.1 Abundance and distribution of leaf wax* n-*alkanes*
409 Long chain *n*-alkanes (C_{25} to C_{35}) were abundant throughout the core.
410 Since sedimentation rate varied in the sediment core, (see fig. 2) we express
411 the abundance of compounds as annual fluxes, i.e. concentrations normalised
412 to sediment amount and deposition time [µg/g dry sediment/year].
413 The total flux of leaf wax *n*-alkanes (summed flux of major (odd-numbered)

long chain *n*-alkanes with 25 to 35 carbons) was stable and low at ca. 0.2 μg/g dry sediment/yr. from 10.1 cal. ka BP to 5.2 cal. ka BP. The flux abruptly increased to values of up to 1.2 μg/g dry sediment/yr. at 5.1 cal. ka BP. A higher flux of leaf wax *n*-alkanes persisted until recent time, however, with few lower values shortly in between (at 4.3 and 0.2 cal. ka BP and between 3.5 to 2.9 cal. ka BP) (Fig. 3c).

The ACL index (concentration weighted average chain length for *n*-alkanes, $\sum n^* Cn / \sum Cn$, where n = number of carbons; here n = 25-35 and Cn = concentration of the *n*-alkane) remained relatively low and varied between 28.6 and 29.4, from 10.1 to 4.8 cal. ka BP. The ACL index showed a slight increasing trend reaching values up to 31.0 from 4 cal. ka BP onwards, with intervening periods of lower values as 28.4, 29.2 and 29.5 at 3.5, 1.3 and 0.3 cal. ka BP, respectively (Fig. 3d).

Between 4.6 and 4.1 cal. ka BP the ACL index varied significantly from 29.8 to 28.2.

3.1.2 Stable carbon isotopic composition of long chain n-*alkanes* ($\delta^{13}C_{wax}$)

Here we report $\delta^{13}C$ values of major *n*-alkanes with 27, 29 and 31 carbon atoms. While overall trends of changes $\delta^{13}C_{wax}$ values were consistent, significant differences in the temporal variations for the individual homologues existed. Over the core, $\delta^{13}C_{wax}$ values showed similar covariance among each other (i.e., *n*-C_{27} with *n*-C_{29} and *n*-C_{31}) (correlation coefficient (r):

r = 0.7, p<0.05). $\delta^{13}C$ values of *n*-C_{27}, *n*-C_{29} and *n*-C_{31} were consistently more negative (–34.5‰ to –27.8‰) from 10.1 to 4.8 cal. ka BP. From 4.8 ka BP onwards the $\delta^{13}C$ values of the individual compounds showed markedly different responses. $\delta^{13}C_{C27}$ values increased towards less negative values (up to –23.8‰) between 4.8 and 4 cal. ka BP and remained at these values until today. $\delta^{13}C_{C29}$ values showed less variability over the core. While more negative (–33.3‰ to –29.1‰) from 10.1 until 5.1 ca. ka BP they increased to values of –26.5‰ at 4.5 cal. ka BP before decreasing again to values around –28.2‰ which remained relatively constant until modern times. $\delta^{13}C_{C31}$ values showed a prominent shift of ~12‰ from –34.8‰ to –22.7‰ after 6 cal. ka BP until 4.5 cal. ka BP and remained less negative (between –22.8‰ and –25.2‰) until 4 cal. ka BP (Fig. 3e), before decreasing again to values around –27.5‰, where they remained until today.

3.1.3 Stable hydrogen isotopic composition of long chain n-*alkanes* (δD_{wax})

Here we report δD values of major *n*-alkanes with 27, 29 and 31 carbon atoms. Throughout the core, δD_{C27} values showed higher covariance with δD_{C29} values (r = 0.9, p<0.05) than with δD_{C31} (r = 0.7, p<0.05). δD_{C31} values were enriched in D relative to the other homologues (ε: enrichment factor; difference of δD values; $\varepsilon_{C31\text{-}C27}$ varied from ~ 35 to 4‰) until 2.3 cal. ka BP (Fig. 3f). δD_{C27} and δD_{C29} values were relatively stable between 9.9 to 5.7 cal. ka BP and varied between –145‰ to –160‰, with few negative values (up to

458 –177‰) in between. These values from δD_{C27} and δD_{C29} showed a shift to more
459 negative values around –172‰ after 5.7 cal. ka BP but became less negative
460 (–136‰) again after 5.1 cal. ka BP. δD_{C27} and δD_{C29} values showed a shift from
461 –175‰ to –135‰ from 5.1 to 4.4 cal. ka BP. These values became relatively
462 stable around –122‰ to –141‰ from 3.5 cal. ka BP onwards (Fig. 3f).
463 Between 4.4 and 4 cal. ka BP these values fluctuated between –145‰ and –
464 180‰.

465
466
467
468
469
470
471
472
473
474
475
476
477
478
479
480
481
482

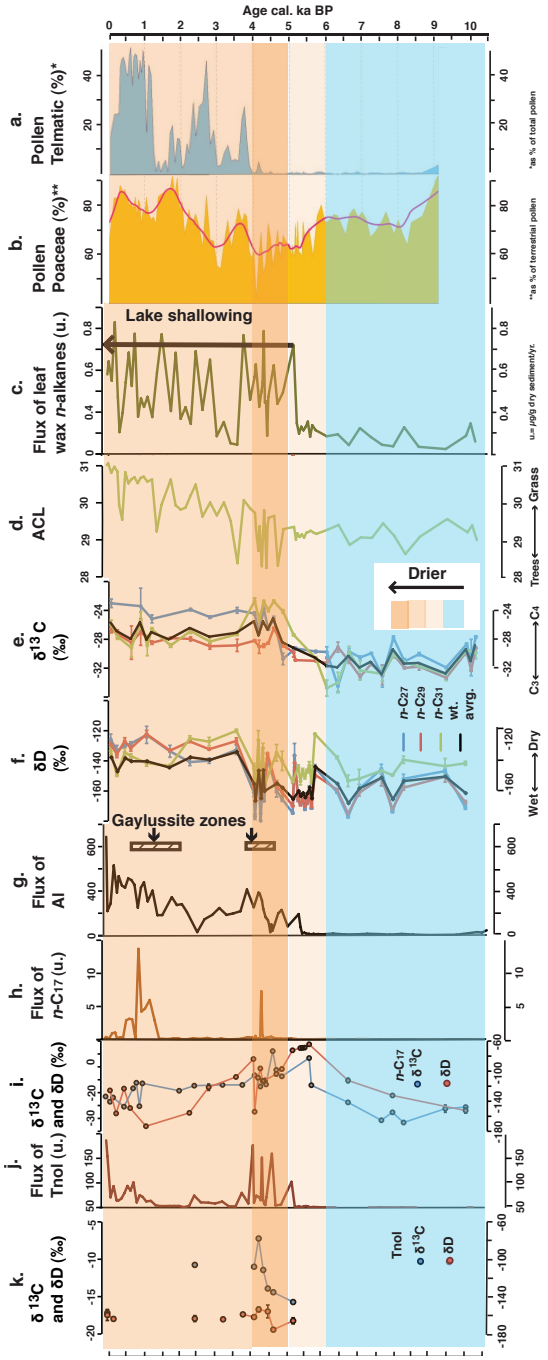

Fig. 3. Flux of major biomarkers and their stable isotopic composition ($\delta^{13}C$, δD) at Lonar Lake during the Holocene, along with other proxies (pollen and Al). a. abundance (%) of pollen from telmatic plants, b. abundance (%) of pollen from Poaceae , c. flux of leaf wax *n*-alkanes, d. ACL, e. $\delta^{13}C$ of long chain *n*-alkanes and concentration weighted average values, f. δD of long chain *n*-alkanes and concentration weighted average values, g. flux of Al (normalised total counts); boxes represent zones where evaporites (gaylussite crystals) were found (modified from Prasad et al., 2014), h. flux of *n*-C_{17}, i. $\delta^{13}C$ and δD of *n*-C_{17}, j. flux of total tetrahymanol (tnol), k. $\delta^{13}C$ and δD of tetrahymanol (tnol). Unit for fluxes of all biomarkers is µg/g dry sediment/year.

3.2 Aquatic biomarkers

3.2.1 Abundance of aquatic biomarkers

The abundance of all aquatic compounds has also been expressed as annual flux, see above. Aquatic biomarkers were virtually absent (or present only in trace amounts) before 6 cal. ka BP.

Similar as observed in modern surface sediments from Lonar Lake (Sarkar et al., 2014) the most abundant biomarkers found in the upper core section were tetrahymanol and the corresponding ketone gammaceranone. Tetrahymanol was absent before 10.1 cal. ka BP and its concentration (and flux) started to increase only after ca. 6 cal. ka BP onwards. Tetrahymanol reached its first maximum abundance at 5.1 cal. ka BP with total (summed for tetrahymanol and gammaceranone) concentration and flux of 1060 µg/g

507 dry sediment and 52.3 μg/g dry sediment/yr., respectively, which persisted
508 until 3.7 cal. ka BP (Fig. 3j). Between 4.6 and 3.9 cal. ka BP total
509 tetrahymanol concentrations and fluxes varied significantly and reached
510 maximum values of up to ca. 1600 μg/g dry sediment and 126 μg/g dry
511 sediment/yr., respectively. After continuing with lower values, tetrahymanol
512 concentration (or flux) started to increase from 1.4 cal. ka BP onwards and
513 reached values of 482 μg/g dry sediment (137 μg/g dry sediment/yr.) in recent
514 times.

515 As in surface sediments (Sarkar et al., 2014), other major biomarkers of
516 aquatic origin in the core included *n*-heptadecane, diploptene, moretene,
517 fernene and carotenoids. Additionally, some compounds were observed in
518 smaller amounts such as phytenes, hopenes, phytols and hopanol.

519 The flux of *n*-heptadecane (*n*-C_{17}) began to increase later compared to that
520 of tetrahymanol, i.e. after ca. 5.1 cal. ka BP. *n*-Heptadecane showed peaks of
521 very high concentration or flux of up to ca. 113 μg/g dry sediment or 13.7 μg/g
522 dry sediment/yr., once at 4.2 cal. ka BP and between 1.3 to 0.5 cal. ka BP
523 (Fig. 3h). During both periods, other short chain *n*-alkanes such as *n*-C_{15}, *n*-
524 C_{16} and *n*-C_{18} were also identified in higher concentrations (up to 5.2, 2.8 and
525 1.1 μg/g dry sediment respectively).

526 The flux of tetrahymanol was up to two orders of magnitude higher
527 compared to that of moretene, diploptene, fernene, *n*-heptadecane and
528 carotenoids, respectively (see online supplementary material for data).

529 Over the period from 6 cal. ka BP until today, the flux of tetrahymanol
530 showed the highest covariance with that of moretene and diploptene
531 (correlation coefficient (r): r = 0.8 and 0.9, $p<0.05$), moderate covariance with
532 that of fernene and phytenes (r = 0.6 and 0.7, $p<0.05$), and no significant
533 covariance with *n*-heptadecane and carotenoids). While *n*-heptadecane and
534 carotenoids showed a different pattern, diploptene, moretene, phytenes and
535 to some extent fernene showed a similar pattern of concentration/flux as of
536 tetrahymanol over the core. *n*-Heptadecane showed a covariance with
537 phytenes (r = 0.4, $p<0.05$) and no significant covariance with carotenoids and
538 fernene.
539
540 *3.2.2 Stable carbon isotope composition ($\delta^{13}C$) of aquatic biomarkers*
541 Although only measured on selected samples, with a focus to cover the
542 transition between early and late Holocene, $\delta^{13}C$ of all the aquatic biomarkers
543 in the core showed less negative values (> –30‰). Further $\delta^{13}C$ of all the
544 aquatic biomarkers in the core did not show any significant covariance with
545 their respective concentrations/fluxes.
546 $\delta^{13}C$ values of tetrahymanol varied between –17.2‰ and –7.2‰. We
547 observed enrichment in ^{13}C (from –15.7‰ to –7.2‰) for tetrahymanol during
548 the period between ca. 5.1 to 4 cal. ka BP (Fig. 3k).
549 $\delta^{13}C$ values of *n*-heptadecane varied between –31.6‰ and –3.9‰.
550 Enrichment in ^{13}C (from –17.1‰ to –6.6‰ and –13.7‰ to –3.9‰) of *n*-

heptadecane was evident after 6 and 5.1 cal. ka BP, with a maximum value of –3.9 ‰ at 4.8 cal. ka BP (Fig. 3i). $\delta^{13}C$ values of *n*-heptadecane did not vary significantly between 4.5 and 0.8 ka BP with an average value of –17.5‰.

3.2.3 Stable hydrogen isotope composition (δD) of aquatic biomarkers

δD values of *n*-heptadecane varied substantially between –173‰ and –64 ‰. As for $\delta^{13}C$ a trend of enrichment in D of *n*-heptadecane was also evident starting from 9.9 cal. ka BP. $\delta^{13}C$ and δD values for *n*-heptadecane showed covariance ($r = 0.8$, $p<0.05$), with less negative $\delta^{13}C$ values corresponding to less negative δD values. The maximum enrichment in D revealed by less negative δD values (–64‰ to –72‰) was observed for *n*-heptadecane during the period between ca. 5.6 to 5.1 cal. ka BP (Fig. 3i). The period after until 4 cal. ka BP was characterized by more negative δD values of *n*-heptadecane, with the most negative value at 4.0 cal. ka BP (–154‰). Afterwards another trend in depletion in D continued until 1.0 cal. ka BP.

δD values of tetrahymanol from 5.1 cal. ka BP onwards, varied between –175‰ and –154‰. A trend of enrichment in D of tetrahymanol was evident from 4.5 to 4.0 cal. ka BP (Fig. 3k).

4. Discussion

4.1 Environmental sensitivities of biomarker based proxies

Based on previous work on modern surface sediments from the Lonar Lake

573 (Sarkar et al., 2014) we have assessed processes that control the distribution
574 of biomarkers in the sediments. For example, strong surficial erosion in the
575 catchment due to sparse vegetation cover may result in higher flux of leaf
576 wax compounds (Sarkar et al., 2014). In addition to higher terrestrial plant
577 source we found that long chain *n*-alkanes are also produced by emergent
578 macrophytes growing in the lake (Sarkar et al. 2014), in accordance to
579 previous findings (Ficken et al., 2000; Gao et al., 2011). Therefore changes in
580 flux of long chain *n*-alkanes in the sediments can result from changes in
581 terrigenous input but also from emergent macrophytes (if present).
582 The average distribution of long chain *n*-alkanes differs between plant
583 types and has been used as a qualitative source vegetation indicator
584 (Eglinton and Eglinton, 2008), although substantial heterogeneity is observed
585 among plant types (Tipple and Pagani, 2012; Bush & McInnerney, 2013;
586 Hoffmann et al., 2013). It appears, that in particular C_4 grasses are
587 characterized by a dominance of longer *n*-alkane homologues: average ACL
588 index values of C_3 trees and C_3 grasses for tropical vegetation from southern
589 Africa have been found to vary between 29.43 ± 0.70 and 30.01 ± 0.93
590 respectively whereas C_4 grasses showed higher ACL values of 31.26 ± 0.98,
591 (Rommerskirchen et al., 2006b). Therefore changes in ACL can potentially
592 record changes in vegetation type such as trees and grasses, which would be
593 prominent for a change between C_3 trees and C_4 grasses.
594 Based on our surface sediment assessment (Sarkar et al. 2014) the most

595 abundant biomarkers of aquatic origin in Late Holocene Lonar Lake
596 (tetrahymanol, diploptene and moretene) were likely derived from a benthic
597 bacterial mat community whereas the major source of *n*-heptadecane seemed
598 to be floating cyanobacterial mats. Among different biological origins of
599 tetrahymanol (Prasad et al., 2014 (suppl. mat.); Sarkar et al., 2014),
600 predatory ciliates appear to be the most relevant in sedimentary records
601 (Mallory et al., 1963; Harvey and McManus, 1991) and in Lonar Lake surface
602 sediments (Sarkar et al., 2014). Human influence and subsequent nutrient
603 supply resulted in increased lake primary productivity, leading to an
604 unusually high concentration of tetrahymanol in modern surface sediments,
605 in particular in nearshore surface sediments. Due to this inhomogeneous
606 deposition of tetrahymanol in modern sediments, lake level fluctuation may
607 potentially affect aquatic lipid biomarker distributions in lacustrine
608 sediments, in addition to source changes.
609
610 *4.2 Environmental sensitivities of stable isotope based proxies*
611 *4.2.1 $\delta^{13}C$ values of leaf wax* n-*alkanes as an indicator of vegetation type and*
612 *aridity*
613 The stable carbon isotopic composition of leaf wax compounds ($\delta^{13}C_{wax}$) is
614 mainly determined by plant's specific photosynthetic pathway (such as C_3
615 and C_4) and the isotopic composition of atmospheric CO_2 (Farquhar et al.,
616 1989). Accordingly $\delta^{13}C_{wax}$ values have been used to reconstruct past changes

617 in the abundance of C_3 vs. C_4 vegetation (Feakins et al., 2005; Eglinton and
618 Eglinton, 2008). C_4 vegetation has an ecological advantage under aridity, high
619 temperature, and low atmospheric pCO_2 conditions over C_3 plants (Eglinton
620 and Eglinton, 2008). Therefore, $\delta^{13}C_{wax}$ records are often used as a proxy for
621 aridity (i.e. Ponton et al., 2012). $\delta^{13}C_{wax}$ values from Lonar Lake sediments
622 should therefore also represent the prevailing hydro-climate in the
623 catchment. However, a possible supply of long chain *n*-alkanes from emergent
624 macrophytes (see above) growing in the lake can potentially affect $\delta^{13}C_{wax}$
625 values in sediments. Since the pollen data (see fig. 3a) indicate that
626 macrophytes (telmatic) appeared only after 4 ka, we argue a possible supply
627 of long chain *n*-alkanes from aquatic sources and as such a possible alteration
628 of $\delta^{13}C_{wax}$ values may be only relevant during the late Holocene.
629
630 *4.2.2 δD_{wax} values as an indicator of P-E balance*
631 The stable hydrogen isotopic composition of leaf wax compounds (δD_{wax}) is
632 determined by the δD values of plant (leaf) water, which in turn is controlled
633 by δD values of environmental water (Sachse et al., 2012), which to a large
634 extent is influenced by the moisture source and precipitation amount
635 (especially in the tropics) (Dansgaard, 1964). Recent research has shown that
636 δD_{wax} values record evaporation in soils (Smith and Freeman, 2006) and
637 transpiration in higher plants (Kahmen et al., 2013a; Kahmen et al., 2013b).
638 Drier conditions therefore should result in D-enriched *n*-alkanes, because of

639 less rainfall and stronger evapotranspiration and vice versa. Therefore δD_{wax}
640 values from Lonar Lake sediments are expected to reflect the isotopic
641 composition of precipitation, modified by evapotranspiration. Additionally
642 differences in photosynthetic pathways (C_3 and C_4) used by plants and plant
643 functional types (such as trees, shrubs or grasses) can lead to distinct δD
644 values among plants growing at the same location under the same climatic
645 condition (Sachse et al., 2012). However changes in vegetation, recorded by
646 palynological proxies, seem not to effect δD_{wax} values at Lonar (for discussion,
647 see section 4.3.2). Therefore we interpret the variability of concentration
648 weighted average δD values of long chain *n*-alkanes rather than individual δD
649 values of long chain *n*-alkanes, as representing largely hydrological changes.
650
651 *4.2.3 Variations in $\delta^{13}C$ values of aquatic biomarkers as a consequence of*
652 *changes in lake water salinity*
653 The carbon isotopic composition ($\delta^{13}C$) of lipids from photosynthesizing
654 aquatic organisms should reflect the carbon isotopic composition of their
655 carbon sources, being mainly dissolved inorganic carbon (DIC). Therefore
656 more positive $\delta^{13}C$ values of cyanobacterial *n*-heptadecane would suggest a
657 ^{13}C enrichment of lake water DIC. Lake water DIC can become enriched in
658 ^{13}C as a result of increased primary productivity, preferentially removing ^{12}C
659 into biomass and enriching ^{13}C in the lake water DIC (Meyers, 2003).
660 However, in Lonar Lake sediments no covariance of flux and $\delta^{13}C$ values for

661 *n*-heptadecane was observed, which would be extected under the above
662 described scenario. Alternatively, cyanobacteria may asses a ^{13}C enriched
663 carbon source such as HCO_3^- present especially in alkaline lakes that are
664 characterized by less negative $\delta^{13}C$ values (Meyers, 2003). Therefore changes
665 in $\delta^{13}C$ values of *n*-heptadecane in Lonar Lake likely reflect lake water
666 salinity and pH related changes in the lake water.
667 Since we interpret tetrahymanol as originating from predatory ciliates
668 occurring in the biocenosis, it can be assumed that the carbon isotopic
669 composition of this lipid would reflect the carbon isotopic composition of the
670 utilized prey (i.e. bacteria and hence their carbon source). The similarity of
671 $\delta^{13}C$ values of tetrahymanol and *n*-heptadecane, more so than with moretene-
672 diploptene, suggests that tetrahymanol-producing ciliates depend, at least
673 partly, on cyanobacteria synthesizing *n*-heptadecane.
674
675 *4.2.4 Variations in δD values of aquatic biomarkers as consequence of change*
676 *in lake water hydrology*
677 The hydrogen isotopic composition of photosynthesizing aquatic organisms
678 depends on the hydrogen isotopic composition of the lake water (Sachse et al.,
679 2012) where less negative δD values would reflect drier conditions through
680 stronger lake water evaporation. However, salinity of the lake water exerts
681 additional control on the hydrogen isotopic composition of cyanobacterial
682 biomarkers via decrease of the isotopic fractionation (between lipid and

683 source water), resulting in even more deuterium enriched lipids (Sachse and
684 Sachs, 2008), therefore amplifying the proxy response to dry conditions.
685 Higher growth rate of organisms can also exert an influence on the hydrogen
686 isotopic composition of certain lipids via increase of isotopic fractionation
687 (between lipid and source water), resulting in strongly deuterium-depleted
688 lipids (Sachs, 2014). Since we observed unusually high concentrations for *n*-
689 heptadecane over the period between 1.3 to 0.5 cal. ka BP, we consider
690 growth rate changes of cyanobacteria could be relevant with respect to the
691 abundance of their biomass deposited in a sediment sample intregrating up
692 to 20 years. Therefore more negative δD values for *n*-heptadecane, at times
693 when *n*-C_{17} concentrations in the sediment were high, might indicate an
694 increase of isotopic fractionation (between lipid and source water), which
695 could result from higher growth rate of their producers.
696
697 *4.3 Holocene hydroclimate changes at Lonar Lake*
698 Based on stable isotope based proxies from biomarkers, we identified three
699 periods of distinct hydrology over the Holocene, which we discuss in the
700 following chapters in detail.
701
702 *4.3.1 The Early Holocene period between 10.1 and 6 cal. ka BP*
703 The Early Holocene period between 10.1 and 6 cal. ka BP was
704 characterized by most negative $\delta^{13}C_{wax}$ values (–34.8‰ to –27.8‰) in the

705 studied sedimentary record, relatively low ACL values (29.4 to 28.6) and
706 lower flux of long chain *n*-alkanes. These data are consistent with the
707 predominance of woody C_3 vegetation in the catchment. Reduced supply of
708 terrigenous material to the lake may imply less erosion in the catchment due
709 to thicker vegetation cover (Sarkar et al., 2014). Concentration weighted
710 average δD_{wax} values of long chain *n*-alkanes were with –158‰ relatively
711 constant during this period. No biomarker evidence for halophilic microbial
712 communities was found in this core section, which is prominent in the
713 biomarker record of the modern lake (Sarkar et al., 2014). $\delta^{13}C$ values of *n*-C_{17}
714 were mostly low, with up to –31.6‰, during this period.
715 Together with previously published data from the Lonar Lake sedimentary
716 record such as pollen and geochemical proxies (Prasad et al., 2014), these
717 data indicate a positive precipitation-evaporation (P-E) balance in the
718 catchment and a higher lake level, as a consequence of an intensified summer
719 monsoon, in agreement with previous studies/ published data from the Indian
720 Ocean basins (Fleitmann et al., 2003; Ponton et al., 2012).
721
722 *4.3.2 The Mid Holocene period between 6 and 4 cal. ka BP*
723 After ca. 6 cal. ka BP, a gradual shift to less negative $\delta^{13}C_{wax}$ values (up to
724 ~12‰), particularly for *n*-C_{31}, indicates a replacement of C_3 vegetation,
725 development of open C_4 grassland consistent with an onset of drier
726 conditions. In addition an increasing flux of biomarkers like tetrahymanol at

727 the same time likely marked the onset of saline conditions in the lake. An
728 increase in lake water salinity/pH was also evident in proxies measured on
729 bulk sediments (less negative $\delta^{13}C_{bulk}$ and $\delta^{15}N$ values) at ca. 6.2 cal. ka BP
730 (Prasad et al., 2014).

731 After the onset of more arid conditions at ca. 6 cal. ka BP, we observed an
732 abrupt increase in the fluxes of leaf wax *n*-alkanes and tetrahymanol at 5.1
733 cal. ka BP (Fig. 3c and j). At 5.2 cal. ka BP an increase in detrital influx of
734 aluminum (Al) (Fig. 3g) and an almost 8-fold increase in sedimentation rate
735 was observed (Prasad et al., 2014). These proxies point to a drastic decrease
736 in the lake level and as such in shoreline proximity of the coring location. The
737 flux of tetrahymanol showed a significant correlation ($r = 0.5$, $p<0.05$) with
738 flux of Al. Therefore we hypothesize that higher transport of lipids from the
739 shore in a smaller lake might be contributing to the large fluxes of these
740 lipids.

741 The highest $\delta^{13}C$ and δD value of *n*-heptadecane (–3.9‰ and –64‰
742 respectively) observed at 5.5 cal. ka BP indicate likely the most alkaline and
743 saline lake conditions and therefore suggest onset of the driest period. The
744 time span between 4.8 and 4 cal. ka was characterized by the least negative
745 $\delta^{13}C$ values for long chain *n*-alkanes (–22.7‰ to –25.2‰) and some less
746 negative average δD_{wax} values (~ –140‰) compared to the early Holocene,
747 suggesting widespread occurrence of C_4 grasses and a negative (P-E) balance
748 in the catchment. As such, this likely was the driest period in central India

749 during the last 10.1 ka. The presence of a distinct zone of evaporitic
750 carbonate (gaylussite) crystals between 4.6 to 3.9 cal. ka BP provides
751 additional support for this interpretation (Anoop et al., 2013, Prasad et al.,
752 2014). Peak concentration and flux of the cyanobacterial biomarker *n*-
753 heptadecane coincided with this drier period (at 4.3 cal. ka BP) and therefore
754 possibly represented events of lake eutrophication, driven by more saline
755 conditions: persistent saline conditions in the lake provided an opportunity
756 for blooming of halophilic cyanobacteria in the ecological niche, reflected by
757 unusually high fluxes of *n*-heptadecane. Carbon isotope values of
758 tetrahymanol showed a steep trend of enrichment in ^{13}C during this period.
759 While tetrahymanol δD values may reflect several hydrogen sources, since it
760 is derived from non-photosynthetic organisms, it is interesting to note that
761 the maximum enrichment in D and ^{13}C of tetrahymanol occurs at the same
762 period (5-4 cal. ka BP), likely also reflecting the effect of lake water salinity
763 on δD of tetrahymanol.

764 An intriguing feature of the period 4.8-4 cal. ka BP are the high amplitude
765 fluctuations and more negative δD_{wax} values between 20‰ and 40‰,
766 sometimes over a period of only ca. 40 years. While short-term fluctuations
767 may be an artifact of the higher sampling resolution during this period,
768 counterintuitively we observed some of the most negative δD_{wax} values during
769 the Holocene (up to –180‰). Since all other organic and inorganic proxy data
770 from that period characterize it as the driest period during the Holocene it is

771 unlikely that these changes in δD_{wax} were a consequence of changes in
772 evapotranspiration, which would result in more positive δD_{wax} (Kahmen et al.,
773 2013b). To achieve a 40‰ difference in plant source water δD (i.e. leaf water)
774 under similar temperatures would require a 50% change in relative humidity
775 (Kahmen et al., 2013b), i.e. contrasting humid and arid phases, which is not
776 supported by any other proxy data during this period. While this transition
777 period coincides with major changes in catchment vegetation cover, in
778 particular a change from predominantly C_3 to C_4 vegetation, this cannot
779 explain the observed more negative δD_{wax} values: Firstly, we observed no
780 correlation between $\delta^{13}C$ and the δD values of individual leaf wax *n*-alkanes
781 (where $\delta^{13}C$ values indicate C_3 vs. C_4 changes), suggesting C_3 vs. C_4
782 differences were not the major controlling factor of changes in δD_{wax}.
783 Secondly, C_3 grasses are characterized by more negative (~20‰) δD_{wax} values
784 compared to C_4 grasses (Sachse at al., 2012), such that the observed
785 vegetation change should have resulted in more positive δD_{wax} values.
786 Thirdly, δD_{wax} values of grasses (C_3 and C_4) have been found to be more
787 negative compared to trees growing at the same site (Hou et al., 2007), but
788 the pollen record suggests the lowest grass (Poaceae) abundance during the
789 Holocene for the transitional period (Fig. 3b). In addition, the overall
790 abundance of grass (Poaceae) pollen (see fig. 3b) suggests grasses were more
791 dominant in the late Holocene compared to the early Holocene, which would
792 have resulted in a decrease of δD_{wax} values (if vegetation would be the only

control) – opposite to what we observed. As such, the observed changes in vegetation cover, in particular during the transitional period, would have diminished the change in sedimentary δD_{wax} values. Therefore, the only explanation for the negative δD_{wax} values during this period supported by multi-proxy data is a change in the isotopic composition of the water source (precipitation) through a change in the dominant moisture source area and/or moisture pathway.

4.3.2.1 Mechanisms for monsoonal moisture source shifts during the mid-Holocene

Here we explore the possible mechanisms for changing moisture sources during the mid-Holocene transitional period between 4.8-4 cal. ka BP. ENSO variability has been shown to alter the isotopic composition of moisture over India, with an up to 2‰ increase in $\delta^{18}O$ values (i.e ~ 16‰ in δD) during El Niño events (Ishizaki et al., 2012). ENSO activity was relatively weak before 4 ka (Moy et al., 2002; Rein et al., 2005; Conroy et al., 2008) but started to increase in frequency and intensity after 4 ka. However, more frequent El Niño events would have resulted in increasing precipitation δD values (Ishizaki et al., 2012) during that time, which is contrary to our observations.

Air masses for modern-day rainfall events in Lonar during different seasons show that in addition to ISM summer monsoonal rainfall sourced mainly from the Arabian Sea (AS), generally drier air is also delivered from

the NW region of India, the Bay of Bengal (BoB), or the NE region of India during the rest of the year (Sarkar et al., unpublished). An enhanced influence of any of these three potential moisture sources (NW, BoB and NE) and/or a decrease of the typical AS sourced ISM rainfall would result in a change in precipitation δD values in the core monsoon zone (CMZ) at Lonar. In order to characterize the seasonality of moisture sources and associated precipitation isotopic values in the CMZ, we analyzed modern day IAEA-GNIP data available from the nearest location Sagar and carried out a back trajectory analysis. Back trajectories of air masses during monsoon months show that more negative precipitation δD values are often associated with a moisture source from the BoB (as in June and August 2004, fig. 4) and/or different moisture pathways passing over larger continental areas (i.e. with a longer transport pathway, such as September 2003, June 2005, see fig. 4).

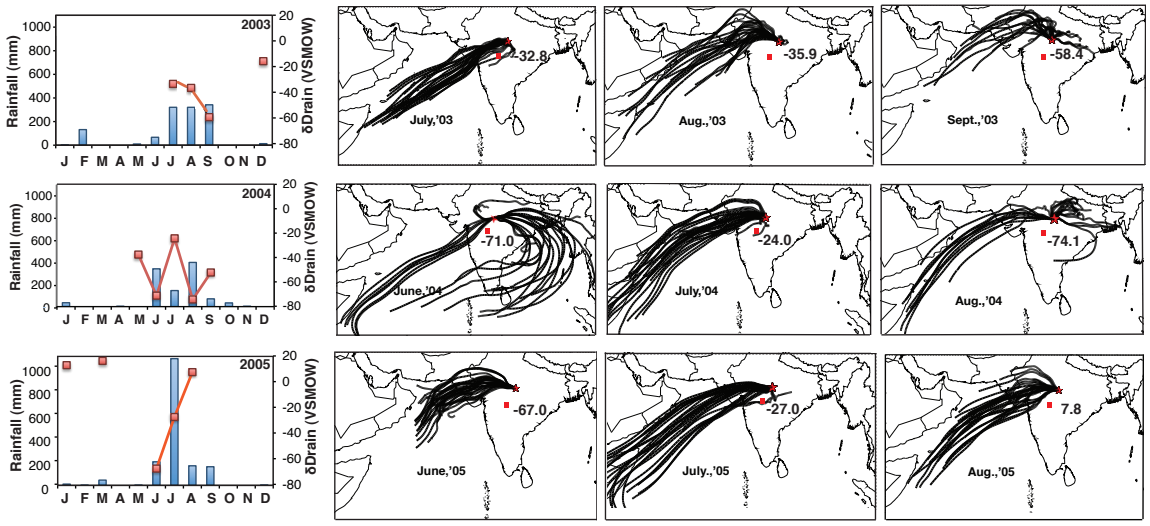

Fig. 4. (a) Monthly rainfall and δD_{rain} variablility at Sagar from 2003 to 2005 (b) Four day

backwards trajectories for air parcels during selected months affecting Sagar (asterisk) during Monsoon, calculated using an ensemble (24 members) of the Air Resources Lab Hysplit Program, to represent moisture source for the region.

Due to the large influx of monsoonal runoff from Himalayan rivers to the BoB the average seawater isotopic composition of the BoB is ~1‰ depleted in $\delta^{18}O$ (or ~8‰ depleted in δD) with respect to the AS (Kumar et al., 2010). An enhanced transport of moisture from the BoB, which occurs mostly today in post-monsoon (Sept. and Oct.) (Sengupta and Sarkar, 2006) would also result in more negative precipitation δD values in the CMZ, due to a longer transport pathway. We therefore hypothesize that during the mid-Holocene transition between 4.8 and 4 ka AS sourced ISM summer rainfall (with less negative δD values) was often strongly reduced and precipitation in the CMZ had different moisture sources/pathways (with more negative δD values). This scenario would result in arid conditions and more negative δD_{precip} (and as such δD_{wax}) values in the CMZ, coherent with our observations.

Possible differences in seasonal monsoonal moisture sourcing during the 4.8 to 4 ka transition should also be evident in other terrestrial (speleothem) records from the region. On the one hand gradually increasing $\delta^{18}O$ values over the Holocene from the Qunf record in Oman, which receives moisture exclusively from the AS, likely reflect the decrease in monsoon strength due to changes in solar insolation. On the other hand, the Mawmluh cave record in NE India is within the reach of BoB sourced moisture, but also receives AS

sourced ISM moisture during the summer months (mean $\delta^{18}O$ of –7.2‰) (Breitenbach et al., 2010). Interestingly the Mawmluh cave record showed an increase in $\delta^{18}O$ values after 6 ka, when Lonar Lake δD_{wax} values decreased (Fig. 5b). If, as we hypothesized above, the AS source became less strong during the mid-Holocene transition on the Indian subcontinent, it would be expected that (summer) $\delta^{18}O$ at Mawmluh becomes more positive, since the moisture transport pathway would be shorter (i.e. mainly BoB moisture would affect NE India), which would be consistent with our hypothesis. We therefore argue, that the period of most negative δD_{wax} during the mid-Holocene at Lonar was a result of changing moisture sources and/or pathways, together with a changed rainfall seasonality, due to a strongly reduced or even completely absent ISM rainfall. As such, the transition from early Holocene wet to late Holocene dry conditions in central India was not gradual, but characterized by relatively rapid changes in hydroclimate conditions, with at times probably a complete failure of summer monsoonal rainfalls, especially between 5 and 4 ka.

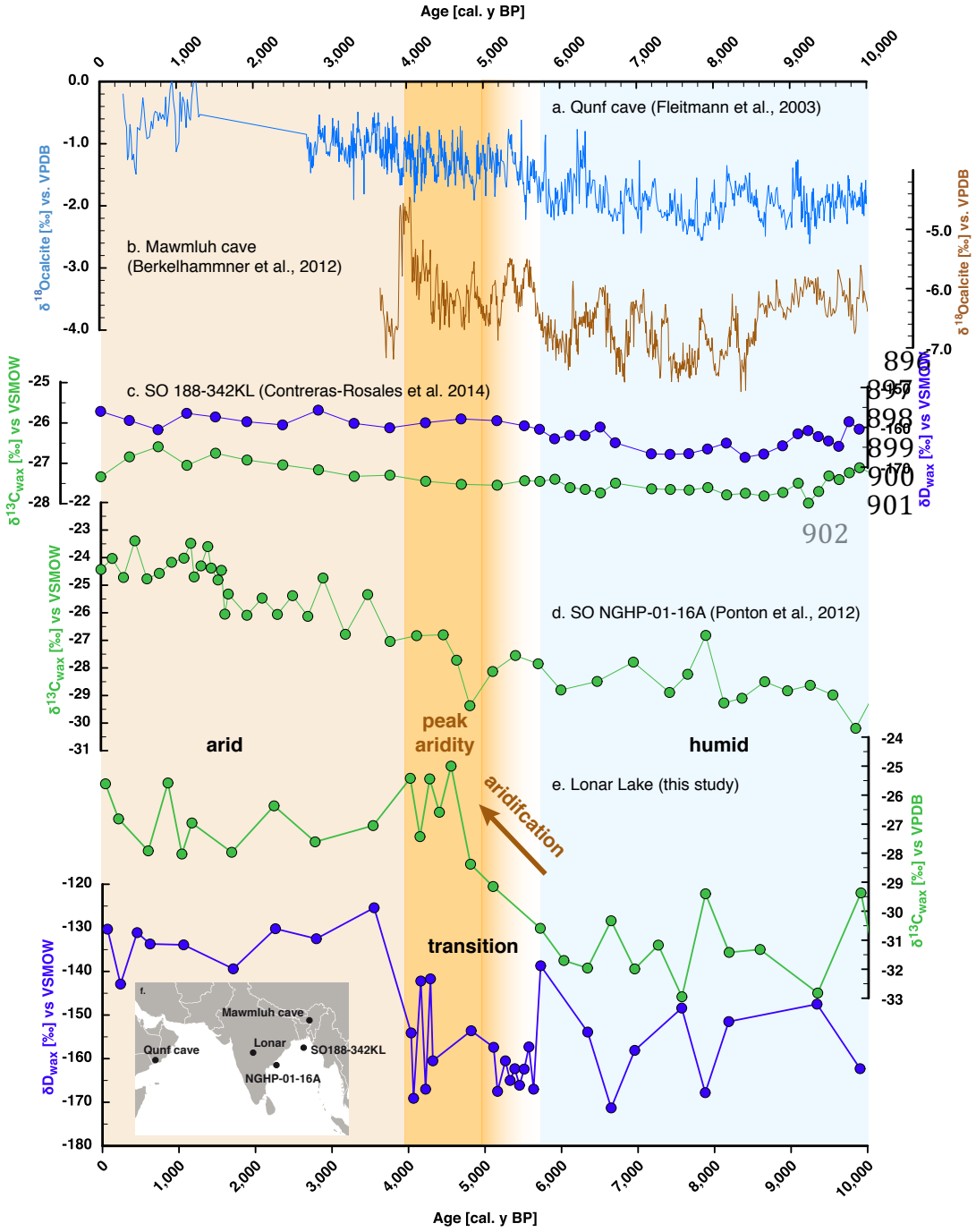
Age [cal. y BP]
a. Qunf cave (Fleitmann et al., 2003)
b. Mawmluh cave
(Berkelhammner et al., 2012)
c. SO 188-342KL (Contreras-Rosales et al. 2014)
d. SO NGHP-01-16A (Ponton et al., 2012)
e. Lonar Lake (this study)
δ18Ocalcite [‰] vs. VPDB
δ13Cwax [‰] vs VSMOW
δDwax [‰] vs VSMOW
arid
peak aridity
humid
aridification
transition
Mawmluh cave
Qunf cave
Lonar
SO188-342KL
NGHP-01-16A

935

936 **Fig. 5.** Holocene ISM variability from Indian monsoon domain; comparison of the records: a.
937 Qunf cave speleothem $\delta^{18}O$ record (Fleitmann et al., 2003), b. Mawmluh cave speleothem
938 $\delta^{18}O$ record (Berkelhammer et al., 2012), c. ice-volume-corrected δD record (weight-averaged
939 for *n*-C_{29} and *n*-C_{31}) and $\delta^{13}C$ record (weight-averaged for *n*-C_{29} and *n*-C_{31}) from sediment core
940 SO188-342KL from northern Bay of Bengal (BoB) (Contreras-Rosales et al., 2014), d. $\delta^{13}C$
941 record (weight-averaged for C_{26}-C_{32} *n*-alkanoic acids) from sediment core NGHP-01-16A
942 offshore from the mouth of Godavari River (Ponton et al., 2012), e. $\delta^{13}C$ record (weight-
943 averaged for *n*-C_{27}, *n*-C_{29} and *n*-C_{31}) and δD record (weight-averaged for *n*-C_{27}, *n*-C_{29} and *n*-
944 C_{31}) for this study, f. locations of the records (inset).
945

946 A Mid-Holocene transition has been recognized throughout the Asian
947 monsoon domain, but its nature (i.e., abrupt vs. gradual) is debated. Morrill
948 et al. (2003) discussed an abrupt (century scale) change in ISM while
949 Fleitmann et al. (2007) argued for gradual weakening of the ISM during the
950 Holocene. Recent leaf wax based stable isotopic records from the Indian
951 Ocean basin (Bay of Bengal) showed a similar overall pattern but with
952 gradual vegetation and hydrological changes during mid-Holocene (Ponton et
953 al., 2012; Contreras-Rosales et al., 2014), likely reflecting the decrease in
954 monsoon strength due to changes in solar insolation during Holocene. These
955 archives, which did not capture the abrupt mid-Holocene transition
956 prominent in our record, represent mainly sediments supplied by the
957 Godavari (Ponton et al., 2012) or Ganges-Brahmaputra rivers (Contreras-
958 Rosales et al., 2014) which do have large, climatologically and ecologically

959 extremely diverse catchments. As such, they are lacking the resolution (in
960 space and time) to record short-term and/or regional variability in moisture
961 sources within the CMZ. In fact, the two available records from the Indian
962 Ocean shelf suggest that the larger the catchment, the smaller is the
963 variability as well as the absolute magnitude of change (Fig. 5). On the
964 contrary, the small catchment and the steep walls of the Lonar crater lake
965 likely result in short residence times of terrestrial leaf waxes in soil. As such
966 short-term variability in changes in the ecosystem as well as the strength of
967 the monsoon can be better captured in those lake sediments.

968 Since the more negative δD_{wax} were observed over a short period only we
969 hypothesize that such instability in atmospheric circulation may only occur
970 under certain threshold conditions of radiative forcing, which pushed the
971 monsoonal circulation system to changes from a relatively stable wet to a
972 stable dry mode. Thus we suggest that orbital induced weakening of the
973 summer solar insolation and associated reorganization of the general
974 atmospheric circulation led to the unstable hydroclimate in the mid-Holocene.
975 Abrupt climatic changes during the mid-Holocene (~4.5 to 5 ka) have also
976 been observed in many records from the Tropical areas supporting the notion
977 of instability of tropical atmospheric circulation patterns. A pronounced shift
978 in ecological conditions during the mid-Holocene (ca. 4 ka) was reported from
979 tropical Africa and South America (Marchant and Hooghiemestra, 2004), and
980 African lakes experienced major lake level drops at ~4.5 ka and did not re-

expand to the previous levels (Gasse, 2000). A decrease in vegetation and an increase in aeolian dust transport in North Africa were suggested as early as ~5.5 ka (deMenocal et al., 2000). New paleohydrological reconstructions from Africa provide evidence for a time-transgressive hydrological change, hypothesizing a combination of decreasing summer insolation and a gradual southward movement of the tropical rainbelt (or the ITCZ) since the mid-Holocene as drivers (Shanahan et al. 2015). Resulting is an aridification in regions from 20°N to 5°N between 5.5 and 3 ka, respectively. Such a scenario should have large-scale consequences, and evidently we observed the onset of aridification at Lonar (20°N) at around 5.5 ka. The ITCZ is moving over the Indian Subcontinent during the ISM, channeling moisture from the AS onto the continent. As such, a more southerly position of the ITCZ during the mid-Holocene transition could have given way to a weaker SW-NE transport of moisture from the AS onto the subcontinent. Since we observed a more stable and isotopically different water source after 4 ka, an alternative explanation is that changes in the variability of the ITCZ position during the mid-Holocene, possibly due solar irradiance passing a threshold value, resulted in stronger moisture source variability.

Our findings of a distinct transitional period between early Holcoene wet and late Holocene dry conditions in the core monsoon zone of central India suggest the possibility of a hydroclimatic instability occurring during mean state changes of the monsoonal system, once an insolation driven threshold

1003 has been passed. This suggests that small changes in solar insolation can be
1004 associated with major hydroclimate/atmospheric changes, a scenario that
1005 may be relevant with respect to future changes in the ISM system.
1006
1007 *4.2.3 The Late Holocene period from 4 cal. ka BP onwards*
1008 From 4 cal. ka BP onwards less negative $\delta^{13}C_{wax}$ values, particularly for *n*-
1009 C_{27} (–25.1‰ minimum) indicate that the catchment vegetation became a
1010 mixed C_3 and C_4 ecosystem, such as a forest with grassy understory. An
1011 almost 40‰ increase in δD_{wax} values relative to the early Holocene, indicates
1012 substantially drier conditions in the catchment. All these proxy data along
1013 with sustained higher flux of tetrahymanol indicate a protracted late
1014 Holocene arid climate, in agreement with previous paleoclimate
1015 reconstructions throughout the ISM realm (Ponton et al., 2012).
1016 Over this period, the flux of leaf wax *n*-alkanes did not show a significant
1017 correlation with the flux of Al, suggesting other factors, in addition to
1018 surficial erosion may have played a role. For example, long chain *n*-alkanes
1019 can also be sourced from emergent macrophytes (Ficken et al., 2000; Gao et
1020 al., 2011), which are common near the alluvial fan in the modern lake
1021 (Sarkar et al., 2014), see also discussion above. Pollen spectra reveal that the
1022 abundance (%) of pollen from aquatic (telmatic) sources increased after 4 cal.
1023 ka BP (Fig. 3a). Therefore the flux of leaf wax *n*-alkanes might have been by
1024 a combination of surficial erosion and macrophyte input after 4 ka. Higher

ACL values during periods of higher aquatic plant pollen abundance (see fig. 3d) indicate that in particular longer chain *n*-alkanes such as *n*-C_{29} and *n*-C_{31} were likely sourced from emergent macrophytes, in agreement with data from the modern emergent macrophyte (*C. laevigatus*) sampled at Lonar (ACL of 31.0) (Sarkar et al., 2014). Increased input from emergent macrophytes, from 4 cal. ka BP onwards could also be the reason for distinct $\delta^{13}C$ values of different long chain *n*-alkane homologues: *n*-C_{29} and *n*-C_{31} showed more negative $\delta^{13}C$ values (~ –27.9‰ and –27.5‰ respectively), while for *n*-C_{27} was less negative (~ –24‰).

Persistent higher fluxes of *n*-heptadecane along with more negative δD values (up to –173‰) may represent another episode of lake eutrophication from 1.4 to 0.8 cal. ka BP, probably reflecting human influence in the catchment area. An increase in human impact was also evident from increase of herb pollen in the sediment and therefore spread of herbaceous taxa in the catchment (Prasad et al., 2014) at that time.

5. Conclusions

We reconstructed the timing and magnitude of Holocene ISM variation and related changes in the hydrology from a high-resolution organic geochemical and stable isotope record from Lonar Lake in central India. We find early Holocene wet conditions due to an intensified monsoon shifted to arid conditions during the late Holocene with a distinct mid-Holocene transition

1047 period between 4.8 and 4 ka.

1048 In particular, we show that:

1049 - The early Holocene (10 to 6 ka) environment at Lonar was humid,
1050 characterized by woody vegetation in the catchment, as evident from more
1051 negative $\delta^{13}C_{wax}$ values and the presence of a fresh water lake. All organic
1052 geochemical proxies indicate a positive P-E balance, coherent with the
1053 intensified ISM.

1054 - From 6 cal. ka BP, an increase in C_4 grass abundance inferred from a
1055 gradual shift of $\delta^{13}C_{wax}$ values coupled with an increase in the abundance of
1056 tetrahymanol, a biomarker for salinity marked the onset of drier conditions
1057 and the establishment of a saline/alkaline lake.

1058 - Multiple lines of evidence (such as maximum C_4 plant abundance, presence
1059 of evaporites) suggested that between 4.8 to 4 cal. ka BP the Lonar region
1060 experienced the driest condition during the Holocene.

1061 - A reduction in aridity from ca. 4 cal. ka BP onwards resulted in mixed (C_3
1062 and C_4) catchment vegetation. An increase in δD_{wax} values of ca. 40‰ relative
1063 to Early Holocene values indicated a protracted late Holocene arid climate
1064 and a saline lake.

1065 The most intriguing feature of our record is the presence of a distinct and
1066 arid mid-Holocene transitional period where we find some of the most
1067 negative δD_{wax} values. We hypothesize that this was due to a change in the
1068 moisture source and/or pathway as well as rainfall seasonality, possibly

connected to a general southward movement of the ITCZ or an increased variability in it's position during the mid-Holocene.

Our data suggest that the mid-Holocene weakening of the ISM was not gradual in central India, but highly variable. As such transitions from one hydrological state into another due to small changes in solar insolation can be associated with major environmental changes/ large fluctuations in moisture source, a scenario that may be relevant with respect to future changes in the ISM system.

Acknowledgements

This research was supported and funded by the DFG-Graduate School 1364/1 "Interactions between Tectonics, Climate and Biosphere in the African–Asian monsoonal region" of the University of Potsdam, funded by the German Science Foundation (DFG) and also DFG Forschergruppe HIMPAC (FOR 1380) (providing the core, radiocarbon dates and pollen data). We thank M. Strecker, acting representative of the Graduate School, for constant support. We also thank all those who provided help during field and laboratory work, especially S. Pinkerneil. We thank S. Polanski for helpful advices in running the HYSPLIT model. Additionally cooperation from the Forest and Wildlife Department of Maharashtra State, India is gratefully acknowledged. D.S. was supported by an Emmy-Noether Grant of the DFG (SA1889/1-1).

References

Anoop, A., Prasad, S., Krishnan, R., Naumann, R., Dulski, P., 2013. Intensified monsoon and spatiotemporal changes in precipitation patterns in the NW Himalaya during the early-mid Holocene. Quaternary International 313-314, 74-84.

Anoop, A., Prasad, S., Plessen, B., Naumann, R., Menzel, P., Basavaiah, N., Weise, S., Gaye, B., Brauer, A., 2013. Palaeoenvironmental implications of evaporative Gaylussite crystals from Lonar lake, Central India. Journal of Quaternary Science 28, 349-359.

APSA Members, 2007. The Australasian Pollen and Spore Atlas V1.0. Australian National University, Canberra. http://apsa.anu.edu.au/.

Basavaiah, N., Wiesner, M.G., Anoop, A., Menzel, P., Nowaczyk, N.R., Deenadayalan, K., Brauer, A., Gaye, B., Naumann, R., Riedel, N., Stebich, M., Prasad, S., 2014. Physicochemical analyses of surface sediments from the Lonar Lake, central India – implications for palaeoenvironmental reconstruction. Fundamental Applied Limnology 184/1, 51–68.

1113 Berkelhammer, M., Sinha, A., Stott, L., Cheng, H., Pausata, F.S.R.,
1114 Yoshimura, K., 2012. An abrupt shift in the Indian monsoon 4000 years ago.
1115 Geophysical Monograph 198, 75–87.
1116
1117 Björck, S., Wohlfarth, B., 2001. ^{14}C chronostratigraphic techniques in
1118 paleolimnology. In: Last, W.M., Smol, J.P. (Eds.), Basin Analysis, Coring, and
1119 Chronological Techniques. In: Tracking Environmental Change using Lake
1120 Sediments, vol. 1. Kluwer, Dordrecht, pp. 205–245.
1121
1122 Bush, R.T., McInerney F.A., 2013. Leaf wax *n*-alkane distributions in and
1123 across modern plants: implications for paleoecology and chemotaxonomy
1124 Geochimica et Cosmochimica Acta 117, 161-179.
1125
1126 Castañeda, I.S., Schouten, S., 2011. A review of molecular organic proxies for
1127 examining modern and ancient lacustrine environments. Quaternary Science
1128 Reviews 30, 2851-2891.
1129
1130 Conroy, J.L., Overpeck, J.T., Cole, J.E., Shanahan, T.M., Steinitz-Kannan,
1131 M., 2008. Holocene changes in Eastern Tropical Pacific climate inferred from
1132 a Galapagos lake sediment record. Quaternary Science Reviews 27, 1166–
1133 1180.
1134

1135 Contreras-Rosales, L.A., Jennerjahn, T., Tharammal, T., Meyer, V., Lückge,
1136 A., Paul, A., Schefuß, E., 2014. Evolution of the Indian Summer Monsoon and
1137 terrestrial vegetation in the Bengal region during the past 18 ka. Quaternary
1138 Science Reviews 102, 133-148.
1139
1140 Cranwell, P.A., Eglinton, G., Robinson, N., 1987. Lipids of aquatic organisms
1141 as potential contributors to lacustrine sediments. 2. Organic Geochemistry
1142 11, 513-527.
1143
1144 Dansgaard, W., 1964. Stable isotopes in precipitation. Tellus 16, 436–468.
1145
1146 deMenocal, P., Ortiz, J., Guilderson, T., Adkins, J., Sarnthein, M., Baker, L.,
1147 Yarusinsky, M., 2000. Abrupt onset and termination of the African Humid
1148 Period: rapid climate responses to gradual insolation forcing. Quaternary
1149 Science Reviews 19, 347-361.
1150
1151 Eglinton, G., Hamilton, R.J., 1967. Leaf epicuticular waxes. Science 156,
1152 1322-1334.
1153
1154 Eglinton, T.I., Eglinton, G., 2008. Molecular proxies of paleoclimatology.
1155 Earth and Planetary Science Letters 275, 1-16.
1156

1157 Feakins, S.J., deMenocal, P.B., Eglinton, T.I., 2005. Biomarker records of late
1158 Neogene changes in northeast African vegetation. Geology 33, 977–980.
1159
1160 Ficken, K.J., Li, B., Swain, D.L., Eglinton, G., 2000. An *n*-alkane proxy for
1161 the sedimentary input of submerged/floating freshwater aquatic
1162 macrophytes. Organic Geochemistry 31, 745-749.
1163
1164 Fleitmann, D., Burns, S.J., Mangini, A., Mudelsee, M., Kramers, J., Villa, I.,
1165 Neff, U., Al-Subbary, A.A., Buettner, A., Hippler, D., Matter, A., 2007.
1166 Holocene ITCZ and Indian monsoon dynamics recorded in stalagmites from
1167 Oman and Yemen (Socotra). Quaternary Science Reviews 26, 170–188.
1168
1169 Fleitmann, D., Burns, S.J., Mudelsee, M., Neff, U., Kramers, J., Mangini, A.,
1170 Matter, A., 2003. Holocene forcing of the Indian monsoon recorded in a
1171 stalagmite from southern Oman. Science 300, 1737–1739.
1172
1173 Fleitmann, D., Burns, S.J., Mangini, A., Mudelsee, M., Kramers, J., Villa, I.,
1174 Neff, U., Al-Subbary, A.A., Buettner, A., Hippler, D., Matter, A., 2007.
1175 Holocene ITCZ and Indian monsoon dynamics recorded in stalagmites from
1176 Oman and Yemen (Socotra). Quaternary Science Reviews 26, 170–188.
1177
1178 Fontes, J.C., Gasse, F., Gibert, E., 1996. Holocene environmental changes in

1179 Bangong Co Basin (Western Tibet): Part 1. Chronology and stable isotopes of
1180 carbonates of a Holocene lacustrine core. Palaeogeography Palaeoclimatology
1181 Palaeoecology 120, 25–47.
1182
1183 Fredriksson, K., Dube, A., Milton, D.J., Balasund, M., 1973. Lonar Lake,
1184 India: An impact crater in basalt. Science 180, 862-864.
1185
1186 Gadgil, S., 2003. The Indian monsoon and its variability. Annual Review of
1187 Earth and Planetary Sciences 31, 429-467.
1188
1189 Gadgil, S., Rajeevan, M., Nanjundiah, R., 2005. Monsoon prediction — why
1190 yet another failure? Current Science 88, 1389–1400.
1191
1192 Gao, L., Hou, J., Toney, J., MacDonald, D., Huang, Y., 2011. Mathematical
1193 modeling of the aquatic macrophyte inputs of mid-chain *n*-alkyl lipids to lake
1194 sediments: Implications for interpreting compound specific hydrogen isotopic
1195 records. Geochimica et Cosmochimica Acta 75, 3781–3791.
1196
1197 Gasse, F., 2000. Hydrological changes in the African tropics since the Last
1198 Glacial Maximum. Quaternary Science Reviews 19, 189-211.
1199

1200 Ghosh, S., Das, D., Kao, S.C., Ganguly, A.R., 2011. Lack of uniform trends
1201 but increasing spatial variability in observed Indian rainfall extremes.
1202 Nature Climate Change 2, 86-91.
1203
1204 Goswami, B.N., Madhusoodanan, M.S., Neema, C.P., Sengupta, D., 2006. A
1205 physical mechanism for North Atlantic SST influence on the Indian summer
1206 monsoon. Geophysical Research Letters 33, L02706, pp. 4.
1207
1208 Gupta, A., Anderson, D., Overpeck, J., 2003. Abrupt changes in the Asian
1209 southwest monsoon during the Holocene and their links to the North Atlantic
1210 Ocean. Nature 421, 354–357.
1211
1212 Harvey, H.R., McManus, G.B., 1991. Marine ciliates as a widespread source
1213 of tetrahymanol and hopan-3ß-ol in sediments. Geochimica et Cosmochimica
1214 Acta 55, 3387-3390.
1215
1216 Hoffmann, B., Kahmen, A., Cernusak, L.A., Arndt, S.K., Sachse, D., 2013.
1217 Abundance and distribution of leaf wax *n*-alkanes in leaves of Acacia and
1218 Eucalyptus trees along a strong humidity gradient in northern Australia.
1219 Organic Geochemistry 62, 62–67.
1220
1221 Ishizaki, Y., Yoshimura, K., Kanae, S., Kimoto, M., Kurita, N., Oki, T., 2012.

1222 Interannual variability of $H_2{}^{18}O$ in precipitation over the Asian monsoon
1223 region. Journal of Geophysical Research 117, D16308, pp. 16.
1224
1225 Jhingran, A.G., Rao, K.V., 1958. Lonar Lake and its salinity. Records of the
1226 Geological Survey of India 85, 313-334.
1227
1228 Hou, J.Z., D'Andrea, W.J., MacDonald, D., Huang, Y., 2007. Hydrogen
1229 isotopic variability in leaf waxes among terrestrial and aquatic plants around
1230 Blood Pond, Massachusetts, USA. Organic Geochemistry 38, 977-984.
1231
1232 Kahmen, A., Hoffmann, B., Schefuß, E., Arndt, S.K., Cernusak, L.A., West,
1233 J.B., Sachse, D., 2013a. Leaf water deuterium enrichment shapes leaf wax *n*-
1234 alkane δD values of angiosperm plants II: Observational evidence and global
1235 implications. Geochimica et Cosmochimica Acta 111, 50-63.
1236
1237 Kahmen, A., Schefuß, E., Sachse, D., 2013b. Leaf water deuterium
1238 enrichment shapes leaf wax *n*-alkane δD values of angiosperm plants I:
1239 Experimental evidence and mechanistic insights. Geochimica et
1240 Cosmochimica Acta 111, 39-49.
1241
1242 Kannenberg, E.L., Poralla, K., 1999. Hopanoid biosynthesis and function in
1243 bacteria. Naturwissenschaften 86, 168-176.

1244

1245 Krishnamurthy, R.V., Syrup, K.A., Baskaran, M., Long, A., 1995. Late-
1246 Glacial Climate Record of Midwestern United-States from the Hydrogen
1247 Isotope Ratio of Lake Organic-Matter. Science 269, 1565-67.

1248

1249 Kumar, B., Rai, S.P., Kumar, U.S., Verma, S.K., Garg, P., Vijaya Kumar,
1250 S.V., Jaiswal, R., Purendra, B.K., Kumar, S.R., Pande, N.G., 2010. Isotopic
1251 characteristics of Indian precipitation. Water Resources Research 46,
1252 W12548, pp. 15.

1253

1254 La Touche, T., 1912. The geology of Lonar Lake. Records of the Geological
1255 Survey of India 41, 266–275.

1256

1257 Malik, N., Bookhagen, B., Marwan, N., Kurths, J., 2012. Analysis of spatial
1258 and temporal extreme monsoonal rainfall over South Asia using complex
1259 networks. Climate Dynamics 39, 971–987.

1260

1261 Mallory, F.B., Conner, R.L., Gordon, J.T., 1963. Isolation of a pentacyclic
1262 triterpenoid alcohol from a protozoan. Journal of the American Chemical
1263 Society 85, 1362-1363.

1264

1265 Marchant, R., Hooghiemstra, H., 2004. Rapid environmental change in

African and South American tropics around 4000 years before present: a review. Earth-Science Reviews 66, 217–260.

Menzel, P., Gaye, B., Basavaiah, N., Prasad, S., Stebich, M., Das, B.K., Nagel, B., Anoop, A., Riedel, N., Wiesner, M., 2013. Impact of bottom water anoxia on nitrogen isotopic ratios and amino acid contributions of recent sediments from small eutrophic Lonar Lake, Central India. Limnology and Oceanography 58, 1061-1074.

Meyers, P.A., 2003. Applications of organic geochemistry to paleolimnological reconstructions: a summary of examples from the Laurentian Great Lakes. Organic Geochemistry 34, 261–289.

Morrill, C., Overpeck, J.T., Cole, J.E., 2003. A synthesis of abrupt changes in the Asian summer monsoon since the last deglaciation. Holocene 13, 465–476.

Moy, C.M., Seltzer, G.O., Rodbell, D.T., Anderson, D.M., 2002. Variability of El Niño/southern oscillation activity at millennial timescales during the Holocene epoch. Nature 420, 162–165.

Nandy, N., Deo, V., 1961. Origin of Lonar Lake and its salinity. TISCO Technical Journal of the Tata iron and steel company Ltd. India 8, 1-2.

1288

1289 Nayar, T.S., 1990. Pollen flora of Maharasthra State. Today and Tomorrows
1290 Publishers, New Delhi.

1291

1292 Ponton, C., Giosan, L., Eglinton, T.I., Fuller, D.Q., Johnson, J.E., Kumar, P.,
1293 Collett T.S., 2012. Holocene aridification of India. Geophysical Research
1294 Letters 39, L03704, pp. 6.

1295

1296 Prasad, S., Anoop, A., Riedel, N., Sarkar, S., Menzel, P., Basavaiah, N.,
1297 Krishnan, R., Fuller, D., Plessen, B., Gaye, B., Röhl, U., Wilkes, H., Sachse,
1298 D., Sawant, R., Wiesner, M.G., Stebich, M., 2014. Prolonged monsoon
1299 droughts and links to Indo-Pacific warm pool: A Holocene record from Lonar
1300 Lake, central India. Earth and Planetary Sciences Letters 391, 171-182.

1301

1302 Rach, O., Brauer, A., Wilkes, H., Sachse, D., 2014. Delayed hydrological
1303 response to Greenland cooling at the onset of the Younger Dryas in western
1304 Europe. Nature Geoscience 7, 109–112.

1305

1306 Rein, B., Lu̇ckge, A., Reinhard, L., Sirocko, F., Wolf, A., Dullo, W.C., 2005. El
1307 Niño variability of Peru during the last 20,000 years. Paleoceanography 20,
1308 PA4003, pp. 17.

1309

1310 Riedel, N., Stebich, M., Anoop, A., Basavaiah, N., Menzel, P., Prasad, S.,
1311 Sachse, D., Sarkar, S., Wiesner, M, 2015. Modern pollen vegetation
1312 relationships in a dry deciduous monsoon forest – a case study from Lonar
1313 Crater Lake, central India. Quaternary International (accepted).
1314
1315 Romero-Viana, L., Kienel, U., Sachse, D., 2012. Lipid biomarker signatures in
1316 a hypersaline lake on Isabel Island (Eastern Pacific) as a proxy for past
1317 rainfall anomaly (1942-2006 AD). Palaeogeography Palaeoclimatology
1318 Palaeoecology 350, 49-61.
1319
1320 Rommerskirchen, F., Plader, A., Eglinton, G., Chikaraishi, Y., Rullkötter, J.,
1321 2006. Chemotaxonomic significance of distribution and stable carbon isotopic
1322 composition of long-chain alkanes and alkan-1-ols in C_4 grass waxes. Organic
1323 Geochemistry 37, 1303–1332.
1324
1325 Sachs, J.P., 2014. Hydrogen Isotope Signatures in the Lipids of
1326 Phytoplankton. In: Holland H.D. and Turekian K.K. (Eds.) Treatise on
1327 Geochemistry, Second Edition, Oxford: Elsevier, vol. 12, pp. 79-94.
1328
1329 Sachse, D., Billault, I., Bowen, G.J., Chikaraishi, Y., Dawson, T.E., Feakins,
1330 S.J., Freeman, K.H., Magill, C.R., McInerney, F.A., van der Meer, M.T.J.,
1331 Polissar, P., Robins, R., Sachs, J.P., Schmidt, H.-L., Sessions, A.L., White,

1332 J.W.C., West, J.B., Kahmen, A., 2012. Molecular Paleohydrology:
1333 Interpreting the Hydrogen-Isotopic Composition of Lipid Biomarkers from
1334 Photosynthesizing Organisms. Annual Reviews of Earth and Planetary
1335 Sciences 40, 221-249.
1336
1337 Sachse, D., Sachs, J.P., 2008. Inverse relationship between D/H fractionation
1338 in cyanobacterial lipids and salinity in Christmas Island saline ponds
1339 Geochimica et Cosmochimica Acta 72, 793-806.
1340
1341 Sarkar, S., Wilkes, H., Prasad, S., Brauer, A., Riedel, N., Stebich, M.,
1342 Basavaiah, N., Sachse, D., 2014. Spatial heterogeneity in lipid biomarker
1343 distributions in the catchment and sediments of a crater lake in central
1344 India. Organic Geochemistry 66, 125–136.
1345
1346 Schwark, L., Zink, K., Lechterbeck, J., 2002. Reconstruction of postglacial to
1347 early Holocene vegetation history in terrestrial Central Europe via cuticular
1348 lipid biomarkers and pollen records from lake sediments. Geology 30, 463-
1349 466.
1350
1351 Sengupta, S., Sarkar, A., 2006. Stable isotope evidence of dual (Arabian and
1352 Bay of Bengal) vapour sources in monsoonal precipitation over north India.
1353 Earth and Planetary Science Letters 250, 511–521.

1354

1355 Shanahan, T.M., McKay, N.P., Hughen, K.A., Overpeck, J.T., Otto-Bliesner,
1356 B., Heil, C.W., King, J., Scholz, C.A., Peck, J., 2015. The time-transgressive
1357 termination of the African Humid Period. Nature Geoscience 8, 140-144.

1358

1359 Sinninghe Damsté, J.S., Kenig, F., Koopmans, M.P., Koster, J., Schouten, S.,
1360 Hayes, J.M., de Leeuw, J.W., 1995. Evidence for gammacerane as an
1361 indicator of water column stratification. Geochimica et Cosmochimica Acta
1362 59, 1895-1900.

1363

1364 Smith, F.A., Freeman, K.H., 2006. Influence of physiology and climate on dD
1365 of leaf wax *n*-alkanes from C_3 and C_4 grasses. Geochimica et Cosmochimica
1366 Acta 70, 1172-1187.

1367

1368 Surakasi, V.P., Antony, C.P., Sharma, S., Patole, M.S., Shouche, Y.S., 2010.
1369 Temporal bacterial diversity and detection of putative methanotrophs in
1370 surface mats of Lonar crater lake. Journal of Basic Microbiology 50, 465-474.

1371

1372 Tierney, J.E., Russell, J.M., Huang, Y.S., Damste, J.S.S, Hopmans, E.C.,
1373 Cohen, A.S., 2008. Northern hemisphere controls on tropical southeast
1374 African climate during the past 60,000 years. Science 322, 252-55.

1375

1376 Tipple, B.J., Pagani, M., 2010. A 35 Myr North American leaf-wax compound-
1377 specific carbon and hydrogen isotope record: Implications for C_4 grasslands
1378 and hydrologic cycle dynamics. Earth and Planetary Science Letters 299,
1379 250–262.
1380
1381 Tipple, B.J., and Pagani, M., 2013. Environmental control on eastern
1382 broadleaf forest species' leaf wax distributions and D/H ratios, Geochimica et
1383 Cosmochimica Acta 111, 64-77.
1384
1385 Tissot, C., Chikhi, H., Nayar, T.S., 1994. Pollen of wet evergreen forest of the
1386 Western Ghats, India. French Institute of Pondicherry, Pondicherry.
1387
1388
1389
1390
1391